

PROCEEDINGS OF SPIE

[SPIDigitalLibrary.org/conference-proceedings-of-spie](https://spiedigitallibrary.org/conference-proceedings-of-spie)

Ultrafast laser-inscribed waveguides in IG2 chalcogenide glass for mid-infrared photonics applications

Helen L. Butcher, David G. MacLachlan, David Lee, Robert R. Thomson, Damien Weidmann

Helen L. Butcher, David G. MacLachlan, David Lee, Robert R. Thomson, Damien Weidmann, "Ultrafast laser-inscribed waveguides in IG2 chalcogenide glass for mid-infrared photonics applications," Proc. SPIE 10535, Integrated Optics: Devices, Materials, and Technologies XXII, 1053514 (23 February 2018); doi: 10.1117/12.2288333

SPIE.

Event: SPIE OPTO, 2018, San Francisco, California, United States

Ultrafast laser-inscribed waveguides in IG2 chalcogenide glass for mid-infrared photonics applications

Helen L. Butcher^{*a}, David G. MacLachlan^b, David Lee^c, Robert R. Thomson^b, Damien Weidmann^a

^aSpace Science and Technology Department (RAL Space), Science and Technology Facilities Council (STFC) Rutherford Appleton Laboratory, Harwell Campus, Didcot, Oxfordshire, OX11 0QX, UK; ^bScottish Universities Physics Alliance (SUPA), Institute of Photonics and Quantum Sciences, School of Engineering and Physical Sciences, David Brewster Building, Heriot-Watt University, Edinburgh, EH14 4AS, UK; ^cScience and Technology Facilities Council (STFC), UK Astronomy Technology Centre, Blackford Hill, Edinburgh, EH9 3HJ, UK.

*helen.butcher@stfc.ac.uk; <https://www.ralspace.stfc.ac.uk/Pages/Laser-Spectroscopy.aspx>

ABSTRACT

We present the first demonstration of ultrafast laser-inscribed waveguides in IG2 chalcogenide glass and their coupling to a mid-infrared quantum cascade laser. The fabrication parameter space has been investigated, resulting in optimized single-mode waveguides that have estimated propagation losses of 1 dB/cm at 7.8 μm . Higher order mode propagation was also observed. The refractive index modification caused by ultrafast laser inscription has been empirically quantified by comparison with modeled waveguide parameters, resulting in $\Delta n = 0.0097\text{--}0.0143$ over the pulse energy range investigated. We will present these findings, alongside our initial investigation into waveguide bend losses, which prepare the building blocks towards mid-infrared evanescent field coupling and integrated sensing applications.

Keywords: ultrafast laser inscription, IG2, chalcogenide, waveguide, mid-infrared.

1. INTRODUCTION

Infrared optical waveguides have numerous potential applications, including across integrated sensing,¹ spectroscopy,² and astrophotonics.³ Substrate-integrated waveguides are of particular advantage due to the low absorption losses, planar platform and, for sensing, the controlled interaction between the waveguide and analyte by design of the waveguide interaction with the material surface. The mid-infrared spectral region is particularly advantageous for molecular sensing as ro-vibrational absorption bands are the strongest across the spectrum, and atmospheric water opacity, and therefore interference, is reduced within the windows at 3–5 and 8–12 μm .

Infrared optical waveguides are a mature technology, with the majority of development in the near-past focused on the telecommunications region in the near-infrared ($< 2.5 \mu\text{m}$). In this spectral region, waveguide components such as evanescent field couplers have been demonstrated,⁴ that offer space-saving advantages over traditional optical-beamsplitters while maintaining low losses and control over the coupling ratio. Evanescent field sensing, typically of the refractive index change in the presence of an analyte, has been exploited for numerous lab-on-a-chip capabilities.² These mature technologies in the near-infrared can be adapted in the mid-infrared spectral region, given appropriate choice of transmissive materials and fabrication techniques suitable for low loss waveguide propagation.

To take advantage of the fundamental ro-vibrational transitions in the mid-infrared spectral region, waveguides suitable for these long wavelength applications need to be developed. Ultrafast laser inscription⁵ has been demonstrated as suitable for rapid-prototyping of waveguides within mid-infrared transmissive materials. Such materials include chalcogenide glasses: ultrafast laser inscription has been used to produce single-mode waveguides in gallium lanthanum sulfide (GLS) at 3.39 μm ,⁴ and single- and multi-mode waveguides have been demonstrated in 75GeS₂-15Ga₂S₃-4CsI-2Sb₂S₃-4SnS (GCIS) at 10.6 μm .⁶

IG2 chalcogenide glass (Ge₃₃As₁₂Se₅₅) has been identified as a suitable candidate for mid-infrared waveguides for atmospheric sensing, as its transmission band covers 1–12 μm , including both atmospheric windows. IG2 is commonly used in astrophotonics applications: initial studies have indicated that IG2 is suitable for ultrafast laser inscription, and transmission grating structures have been successfully demonstrated in the material.⁷ The purpose of this study is to characterize the ultrafast laser inscription parameter space for fabrication of single-mode waveguides in IG2, via

fabrication and characterization of a wide range of waveguides, and to verify the waveguide performance by detailed theoretical modelling. To move toward the development of structures enabling sensing applications, an understanding of the performance of waveguides in IG2 is necessary, including propagation and bend losses; we also present fabrication and characterization of bend structures in IG2.

2. FABRICATION OF WAVEGUIDES

The waveguides were fabricated using the ultrafast laser inscription technique, which is described in detail elsewhere.⁴ In short, a circularly-polarized, short-pulsed laser beam is focused within the volume of a bulk material, creating a refractive index modification at the focal point of the beam. The bulk material is moved such that the beam ‘draws’ waveguide structures within the material. Each waveguide is made up of a single vertical layer, and is formed using the ‘multiscan’ technique,⁵ where the horizontal extent of the waveguide is defined by a number of adjacent inscription paths spaced 0.3 μm apart. The parameters used to create the waveguides described here are as follows: laser wavelength = 1030 nm; pulse duration \approx 355 fs; repetition rate = 500 kHz; waveguide depth from surface of substrate \approx 150 μm ; inscription lens = 0.55 NA; translation speed = 10 mm/s. A schematic of the fabrication process is shown in Figure 1(a).

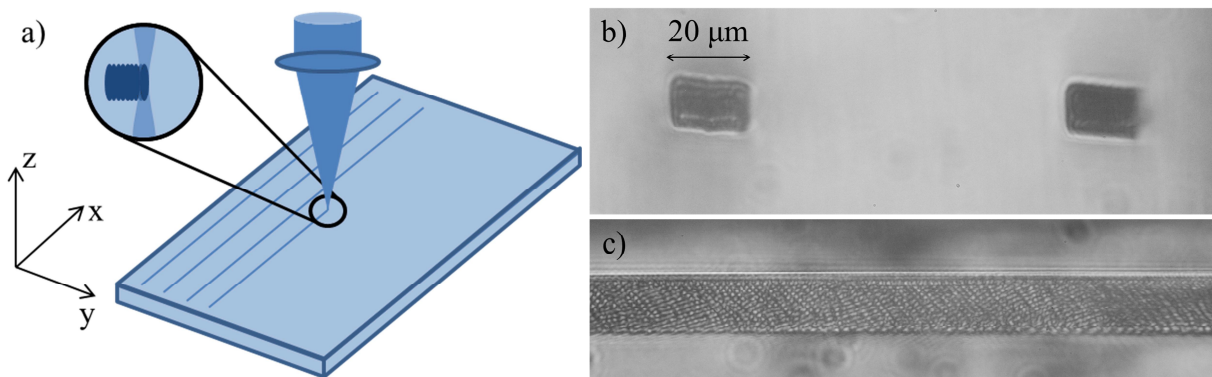


Figure 1. (a) Schematic of ultrafast laser inscription process. The focal point of the inscription beam is static, while the sample is moved in three dimensions to inscribe the waveguides. The multiscan technique is used to create waveguides using multiple horizontal inscribed lines. The vertical extent of the waveguide consists of a single scan, and is controlled by the focal point characteristics and changes to the inscription pulse energy. (b) Microscope image of fabricated waveguide facet. (c) Top view of fabricated waveguide within chip. Images (b) and (c) were taken using a DSLR camera with the infrared filter removed, mounted on a microscope system.

The waveguides inscribed were 20 mm long, with a range of pulse energies (10.44–16.62 nJ) and horizontal waveguide cross-sections (15–23.4 μm). This range of pulse energies and horizontal cross-sections allowed a range of single- and multi-mode waveguide cross-sections to be fabricated for test. Figures 1(b) and (c) show microscope images of typical waveguide facets and top view. Waveguides have a center-to-center separation of \approx 100 μm , to eliminate coupling between adjacent structures (Figure 1(b)). The waveguides are written across the full width of the sample, which may result in some tapering at the input and output regions due to proximity to the sample edge. There is no observed damage to the sample facets caused by inscription.

3. WAVEGUIDE CHARACTERIZATION

Waveguides were characterized to investigate both output mode profiles and throughput power of the waveguide. The laser used was a distributed feedback pulsed quantum cascade laser (QCL) with output at 7.83 μm ; the pulse duration was 50 ns with a repetition rate of 400 kHz. The output collimated laser beam was focused on the waveguide input facet using a microscope objective, to achieve an input spot size close to the dimensions of the waveguide facet. A schematic of the characterization setup is shown in Figure 2. The output mode profile indicates if multi-mode guiding occurs, which is an indicator that the waveguide has sufficient Δn and waveguide cross-section to support a higher order mode. The throughput power of the waveguide was observed to ensure consistency between waveguides, and to allow waveguides with fabrication errors and thus inconsistent losses to be discounted.

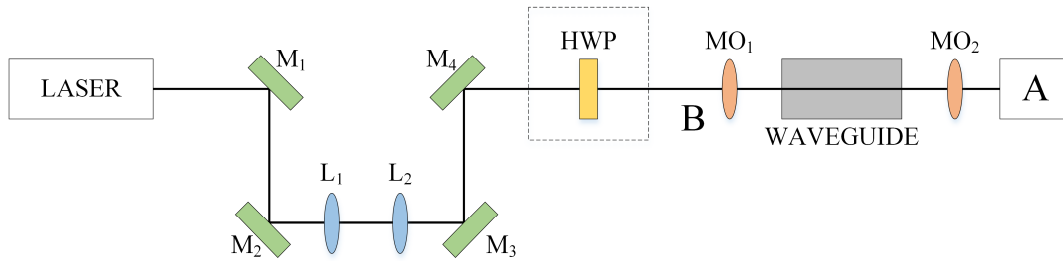


Figure 2. Characterization setup. Mirrors M_{1-4} (green) are beam steering mirrors. Lenses L_1 and L_2 (blue) form a collimated beam with beam diameter of 3 mm. Microscope objectives MO_1 and MO_2 (orange) couple the laser to the waveguide (focal length = 6 mm), creating a beam waist of approx. $10\ \mu\text{m}$ at the input facet. The beam profile is measured using a camera at position 'A', and waveguide throughput is calculated by differential measurement of the power at 'A' and 'B'. HWP (yellow) is a half-wave plate, inserted to control the polarization state of the characterization beam.

Figure 3 shows example mode profiles observed at position 'A' in Figure 2, for two waveguides with different fabrication parameters: (a) shows the single-mode profile obtained for the waveguide with horizontal cross-section $19.8\ \mu\text{m}$, and inscription pulse energy $14.3\ \text{nJ}$; and (b) shows the higher order TE_{21} profile obtained at the output of the waveguide written with $23.4\ \mu\text{m}$ cross-section and $16.1\ \text{nJ}$ pulse energy. All waveguides exhibited single-mode guiding. As the waveguide dimensions and pulse energy increase, the higher order mode output becomes more pronounced; this is due to the larger size of the waveguide structure for constant wavelength, and also the increased refractive index contrast achieved for higher inscription pulse energy.

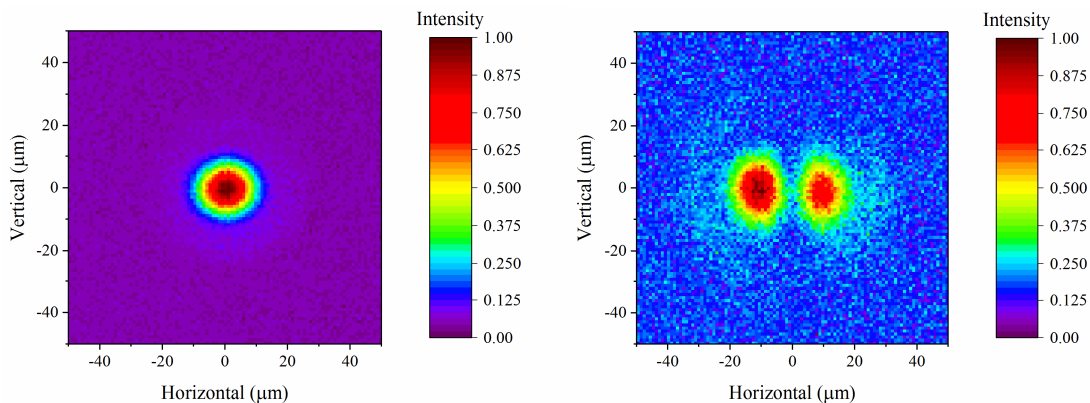


Figure 3. Example mode profiles of IG2 waveguides. (a) Single-mode TE_{11} profile, horizontal waveguide cross-section = $19.6\ \mu\text{m}$, pulse energy = $14.3\ \text{nJ}$. (b) Higher order mode TE_{21} waveguide output, horizontal waveguide cross-section = $23.4\ \mu\text{m}$, pulse energy = $16.1\ \text{nJ}$.

The measured throughput of these waveguides was close to $P_{\text{out}} = 30\%$ total transmission in the most efficient case, with transmission measured through both microscope objectives and the waveguide itself. Reflection loss from the IG2 facets, loss due to the numerical aperture (NA) mismatch of the microscope objective and the waveguide, and losses due to imperfections of the anti-reflection coated microscope objectives contribute to an overall maximum transmission throughput of $P_{\text{in}} = 47.4\%$. Having taken account of these coupling losses, the waveguide propagation loss is therefore determined to be $0.99\ \text{dB/cm}$. This is comparable to the best propagation losses observed for similar GLS ultrafast laser-inscribed waveguides ($0.8\ \text{dB/cm}$).⁴

The measurement repeatability was estimated by multiple throughput measurements of the same waveguide; throughput power was observed to vary by $\pm 0.65\%$. The measurement error on the propagation loss is therefore $0.99 \pm 0.02\ \text{dB/cm}$. Similarly, the manufacturing repeatability was determined by measuring five waveguides written with identical fabrication parameters. The observed throughput power varied by $\pm 6.2\%$ among the five devices under test, indicating a variability ten times larger than the measurement error; this value is dominated by a single outlier that skews the statistics. Manufacturing uncertainty clearly dominates this small set of devices. This is thought to be due to local inconsistencies in the bulk material, cleanliness of the samples during manufacture, and/or local damage to the

waveguide facets. Further work is required to characterize the sources of manufacturing variability and produce waveguides with more consistent optical properties.

4. THEORETICAL VERIFICATION

Detailed modeling work was undertaken to interpret these waveguide fabrication results. In particular, work was undertaken to understand the relationship between waveguide propagation and the fabrication parameters, specifically the refractive index modification introduced on inscription. Modeling was carried out using the FIMMWAVE modeling tool, which allows analytical or numerical solving of the Maxwell's equations describing the waveguide structure.

In this instance, FIMMWAVE was used to calculate the effective refractive index of the higher order TE₂₁ mode of waveguide structures with square facet cross-section. An effective refractive index larger than that of the surrounding medium (IG2 $n = 2.5032$ at $7.83 \mu\text{m}$) indicates that the higher order mode is supported and can propagate within the waveguide. Figure 4(a) shows contours indicating the effective index of the TE₂₁ mode as a function of the refractive index modification and the waveguide cross-section. Colored contours indicate that the mode is supported.

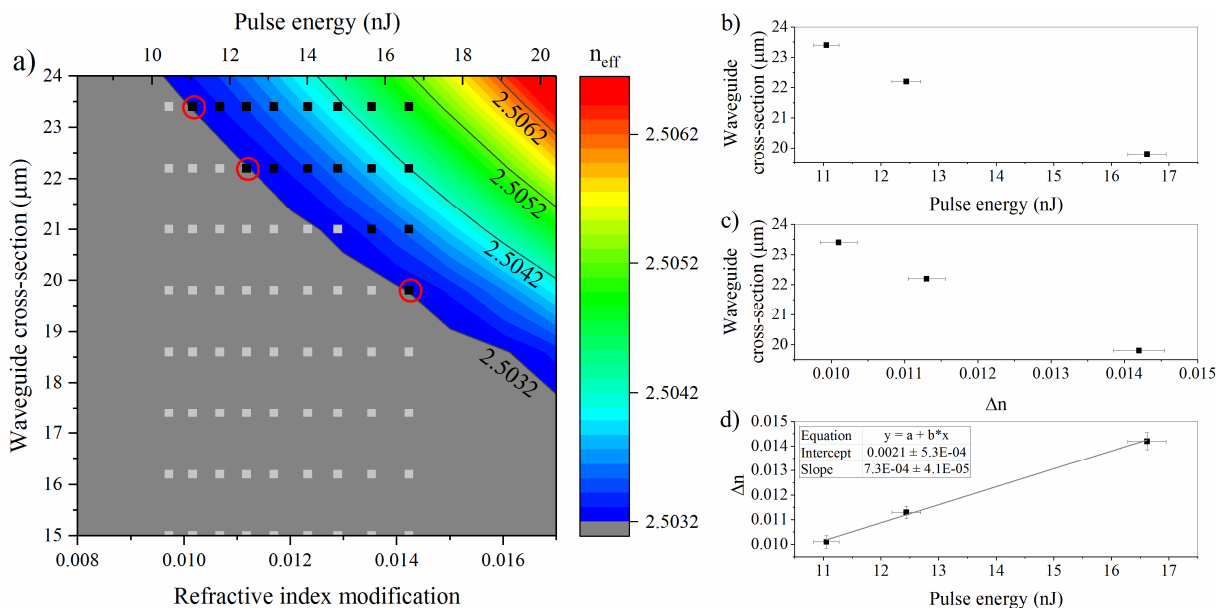


Figure 4. (a) Modeled (colored contour) and measured (grey and black points) refractive index modification, as a function of waveguide horizontal cross-section and fabrication pulse energy. Grey points denote waveguides that only support the fundamental mode, while black points denote waveguides that were observed to support the TE₂₁ higher order mode. (b) Relation between pulse energy and waveguide cross-section for highlighted waveguides (circled red). (c) Relation between Δn and waveguide cross-section, from modeled FIMMWAVE expectation of higher order mode cut-on. (d) Relationship and fit, including errors, between inscription pulse energy and Δn .

The black points overlaying this plot indicate the waveguide horizontal cross-section and pulse energy for which the TE₂₁ higher order mode was observed during the measurement phase. The grey points indicate where only the fundamental mode was observed.

To calculate the dependence of refractive index modification on laser pulse energy, the cut-on of the higher order mode was compared for both measured waveguides and model. Three waveguides were identified, where the TE₂₁ mode was first observed at the waveguide output for a specific waveguide cross-section; these are highlighted in red in Figure 4(a). There is an additional data point that falls within the higher order mode region of the plot, but for which higher order mode output was not observed ($21 \mu\text{m}$ cross-section, $\Delta n = 0.013$). This point was discarded from the calculation, as non-observance of the higher order mode is likely caused by manufacturing repeatability error, as described above.

The waveguide cross-section and pulse energy (E) are well-known fabrication parameters; a plot showing the values for this waveguide subset is shown in Figure 4(b). The error bar shows the error in fabrication pulse energy; the laser pulse

energy fluctuates by $\pm 2\%$ during inscription. The waveguide cross-section has a very small error of $\pm 0.2 \mu\text{m}$ associated with it, due to the air-bearing stage accuracy; this is not shown as it falls within the data points on this scale.

Similarly, the model predicts the refractive index modification required for the higher order mode to be supported within the waveguide structure; the points for this subset are shown in Figure 4(c). These were obtained from the '2.5032' contour in Figure 4(a). The inscription pulse energy and inscribed Δn can therefore be equated for known waveguide cross-sections. This data is shown in Figure 4(d). The linear fit, assumed to be relevant over a small extent of pulse energies (local linearization), results in the relation:

$$\Delta n = 0.00073E + 0.0021 \quad (1)$$

This relation was used to calculate the 'pulse energy' scale on the top of Figure 4(a), for visual representation of this data. The range of refractive index modification achieved across this fabrication pulse energy range was $\Delta n = 0.0097\text{--}0.0142$. The error in refractive index modification was also calculated, based crudely on the half-distance between adjacent pulse energies; this error varied between ± 0.00022 to ± 0.00035 across the range.

This method provides an indication of the relationship between inscription pulse energy and refractive index modification. While the linear fit in Figure 4(d) falls within the error bounds on the individual waveguides, ULI is a non-linear process, and thus a non-linear relation between inscription pulse energy and refractive index modification is expected. This is corroborated by the non-zero intersection point of the linear fit. Further data points around this transition region between single- and multi-mode guiding structures would enable the relationship between inscription pulse energy and refractive index modification to be better understood.

5. BEND WAVEGUIDES

The long-term aim of this work is to develop mid-infrared waveguides and photonic elements such as cross-couplers and evanescent field sensors that are suitable for mid-infrared astrophotonics and sensing applications. These devices will contain bent waveguide sections. In order to experimentally characterize bent sections, waveguides containing bend sections of various widths and lengths were fabricated, to determine the maximum bend dimensions that produce waveguides with reasonable transmission losses.

Inscribed bends had a sine-squared form,⁴ and were inscribed in the center of the 20 mm long waveguide chip with straight input and output waveguides extending to the edges of the sample. All bends were inscribed in the same horizontal plane, so the TM (vertically polarized) mode is least affected by the bend structure. The bend had form $y(x) = A \sin^2(2\pi x/4L_c)$, where A is the bend width, and L_c is the bend length,⁴ as shown in Figure 5. Bend widths ranged from 40–130 μm , and bend lengths from 2–9 mm; the length of each waveguide bend structure was 20 mm in total once input and output waveguide sections were included. All waveguides were inscribed with horizontal cross-section of 19.8 μm , and pulse energy of 12.53 nJ; all waveguides are expected to be single-mode, as indicated in Figure 4(a). The waveguide throughput power was used as an indicator of efficiency of the bend structure.

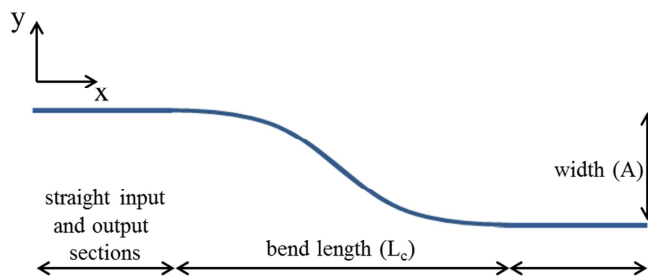


Figure 5. Schematic of the bend structure, showing variables 'width' and 'bend length' varied during this exercise.

The contour plot in Figure 6(a) shows the measured transmission of the waveguides in the TM polarization state, as a function of the inscribed waveguide bend length and width. The transmission is normalized to the maximum throughput transmission of a co-located straight waveguide, to indicate the additional losses introduced by the bend structure alone, in addition to the propagation losses of a 20 mm long waveguide.

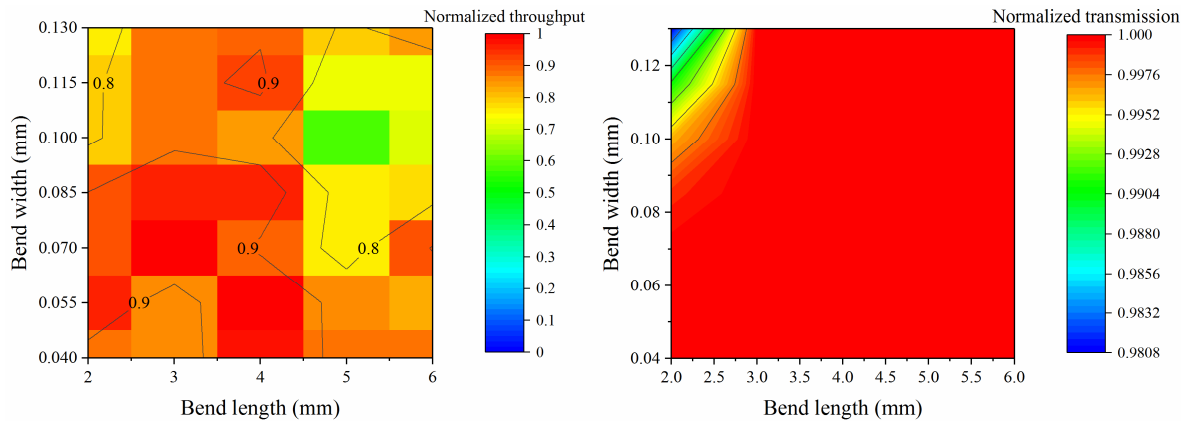


Figure 6. (a) Measured normalized throughput of bend waveguide structures, showing impact of bend only. (b) Analytical model of bend waveguide structures. Note different color scales.

The measured data shows significant variation, of around 10–20%, in the normalized throughput power, throughout the bend parameter space. Conversely, the analytic model of the waveguide structure (Figure 6(b)), based on the waveguide geometry simplified to a simple circular bend structure, indicates a variation in waveguide throughput dependent on bend geometry expected to be $\approx 2\%$ for identical parameter space. The measurements are clearly dominated by manufacturing reproducibility and cannot bear any conclusive interpretation. They do, however, indicate that either the manufacturing variability must be significantly reduced, or the bend parameter space under scrutiny needs to be extended to achieve more significant throughput variations and thus better understanding of the bend parameter space.

An example output mode profile from a waveguide containing a bend structure is shown in Figure 7.

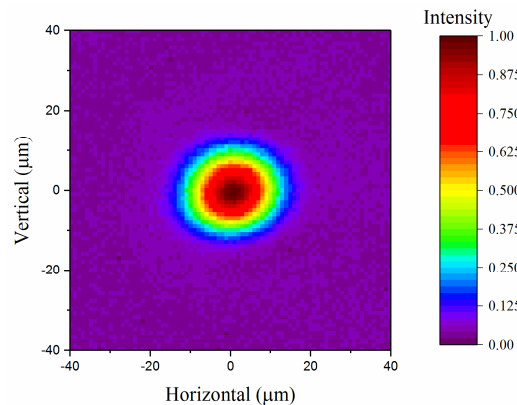


Figure 7. Output mode profile of a bend waveguide. Bend profile is 100 μm wide and 4 mm long, with a waveguide that has 19.8 μm horizontal cross-section, written with pulse energy 12.53 nJ. The waveguide was characterized with vertical linearly-polarized input from the QCL.

Qualitatively, the inscribed bend structures are clearly working, and deliver a clean, single-mode spatial mode output for the inscription parameters investigated, making them suitable for integration into more complex waveguide geometry.

6. CONCLUSION

Ultrafast laser-inscribed waveguides suitable for mid infrared applications have been demonstrated in IG2 chalcogenide glass for the first time, using QCL coupling to study their properties. Waveguide propagation losses are estimated to be close to 1 dB/cm at 7.8 μm . Theoretical modelling of the waveguide structures indicates that a refractive index modification between $\Delta n = 0.0097\text{--}0.0142$ was achieved on inscription across the range of pulse energies investigated.

In addition, waveguide bend structures were fabricated in IG2. The bend structures investigated allowed input and output waveguides to be separated laterally by more than 100 μm , across bend lengths as short as 2 mm, whilst introducing minimal additional propagation loss to the structure.

These advances will be used in future for the design of waveguide components for astrophotonics and mid-infrared sensing applications.

REFERENCES

- [1] Kasberger, J., Fromherz, T., Saeed, A. and Jakoby, B., "Miniaturized integrated evanescent field IR-absorption sensor: Design and experimental verification with deteriorated lubrication oil," *Vib. Spectrosc.* 56, 129-135 (2011).
- [2] Lavchiev, V. M. and Jakoby, B., "Photonics in the mid-infrared: challenges in single-chip integration and absorption sensing," *IEEE J. Sel. Top. Quant.* 23(2), 8200612 (2017).
- [3] Hsiao, H.-K., Winick, K. A., Monnier, J. D. and Berger, J.-P., "An infrared integrated optic astronomical beam combiner for stellar interferometry at 3–4 μm ," *Opt. Express* 17(21), 18489-18500 (2009).
- [4] Arriola, A., Mukherjee, S., Choudhury, D., Labadie, L. and Thomson, R. R., "Ultrafast laser inscription of mid-IR directional couplers for stellar interferometry," *Opt. Lett.* 39(16), 4820-4822 (2014).
- [5] Arriola, A., Gross, S., Ams, M., Gretzinger, T., Le Coq, D., Wang, R. P., Ebendorff-Heidepriem, H., Sanghera, J., Bayya, S., Shaw, L. B., Ireland, M., Tuthill, P. and Withford, M. J., "Mid-infrared astrophotonics: study of ultrafast laser induced index change in compatible materials," *Opt. Mater. Express* 7(3), 698-711 (2017).
- [6] Ródenas, A., Martin, G., Arezki, B., Psaila, N., Jose, G., Jha, A., Labadie, L., Kern, P., Kar, A. and Thomson, R., "Three-dimensional mid-infrared photonic circuits in chalcogenide glass," *Opt. Lett.* 37(3), 392-394 (2012).
- [7] Lee, D., MacLachlan, D. G., Butcher, H. L., Brownsword, R. A., Weidmann, D., Cunningham, C. R., Schnetler, H. and Thomson, R. R., "Mid-infrared transmission gratings in chalcogenide glass manufactured using ultrafast laser inscription," *Proc. SPIE* 9912, 91222X (2016).